# ORIGINAL RESEARCH

White Adipose Tissue Autophagy and Adipose-Liver Crosstalk Exacerbate Nonalcoholic Fatty Liver Disease in Mice

Sadatsugu Sakane, Hayato Hikita, Kumiko Shirai, Yuta Myojin, Youichi Sasaki, Shinnosuke Kudo, Kenji Fukumoto, Naoki Mizutani, Yuki Tahata, Yuki Makino, Ryoko Yamada, Takahiro Kodama, Ryotaro Sakamori, Tomohide Tatsumi, and Tetsuo Takehara

Department of Gastroenterology and Hepatology, Graduate School of Medicine, Osaka University, Osaka, Japan
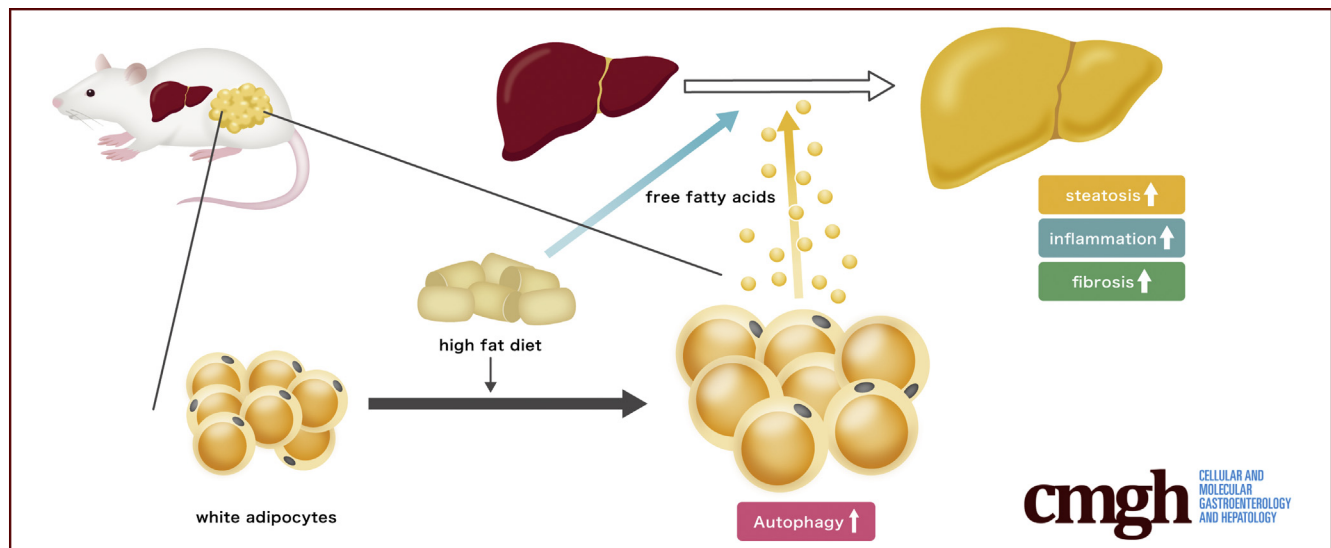
SUMMARY

Autophagy was enhanced in white adipose tissues of mice fed a high-fat diet. The suppression of autophagy in white adipose tissue ameliorated liver steatosis, inflammation, and fibrosis. Adipocyte autophagy contributes to the liver pathogenesis of nonalcoholic fatty liver disease.

BACKGROUND & AIMS: Although nonalcoholic fatty liver disease (NAFLD) is closely associated with obesity, the role of adipose tissue in NAFLD is not well-understood. Because autophagy has been reported to be involved in the degradation of lipid droplets, we investigated the role of adipose tissue autophagy in the liver pathogenesis of NAFLD.

METHODS: C57BL/6J mice and adipocyte-specific Atg7-knockout mice (Adipoq-Atg7 KO mice) were fed a high-fat diet (HFD).

RESULTS: HFD feeding for up to 4 months increased both inguinal and epididymal white adipose tissue (iWAT and eWAT, respectively; the former represents subcutaneous fat, and the latter represents visceral fat) in mice. After HFD feeding, autophagy flux in both types of white adipose tissue was increased, and the levels of Rubicon, a negative autophagy regulator, were decreased, suggesting autophagy promotion.

Adipoq-Atg7 KO mice exhibited suppressed autophagy in both iWAT and eWAT. Adipocyte-specific Atg7 KO enhanced HFD-induced iWAT hypertrophy. On the other hand, eWAT levels in Adipoq-Atg7 KO mice were increased after 1 month of HFD feeding but decreased after 4 months of HFD feeding compared with those in wild-type controls. Cleaved caspase 3 and JNK pathway protein expression in eWAT was increased without cytokine elevation in Adipoq-Atg7 KO mice fed an HFD compared with wild-type mice fed an HFD. Adipocyte-specific Atg7 KO decreased serum free fatty acid levels and ameliorated HFD-induced steatosis, liver inflammation, and fibrosis.

CONCLUSIONS: Autophagy was enhanced in the white adipose tissues of mice fed an HFD. Autophagy inhibition in white adipose tissues ameliorated the liver pathology of NAFLD via adipose-liver crosstalk. *(Cell Mol Gastroenterol Hepatol 2021;12:1683–1699; https://doi.org/10.1016/j.jcmgh.2021.07.008)*

Keyword: Nonalcoholic Steatohepatitis.

Nonalcoholic fatty liver disease (NAFLD) is the most common chronic liver disease. NAFLD may progress to nonalcoholic steatohepatitis (NASH), and patients with NASH constitute a high-risk group for liver carcinogenesis.[1] Although there is a need for effective therapeutic agents for NAFLD and NASH, none as yet exist. Fifty percent

of NAFLD patients and 80% of NASH patients are obese.[2] In addition, visceral fat obesity has been reported to be a risk factor for inflammation and fibrosis in steatohepatitis.[3,4] The appearance of insulin resistance, changes in adipocytokines, and increased inflammatory cytokines due to obesity adipocytes are associated with the liver pathology of NAFLD.[5] Thus, intervention in adipose tissue may be an effective treatment for NAFLD/NASH via adipose-liver crosstalk.

Autophagy is an intracellular degradation system that is important for the maintenance of cell homeostasis. Recently, autophagy has been reported to be involved in the degradation of lipid droplets in hepatocytes.[6] Autophagy is thought to play an important role in NAFLD, and there have been several reports that hepatocyte autophagy is suppressed in NAFLD.[7] We have previously reported that autophagy is suppressed in the liver via increases in Rubicon,[8] which is an autophagy-inhibiting protein.[9]

Several studies have suggested that adipose tissue autophagy is involved in adipocyte differentiation[10] and is important for beige adipocyte maintenance.[11] Recently, Yamamuro et al[12] reported that the up-regulation of autophagy and decreases in Rubicon in aged adipocytes contribute to metabolic dysfunction. However, the changes in autophagy that occur in obesity and the significance of adipose tissue autophagy in the pathogenesis of NAFLD are unclear.

In this study, we investigated changes in adipose tissue autophagy in a mouse model of NAFLD and the effects of these changes on the liver pathogenesis of NAFLD.

Results

High-Fat Diet Intake Promotes Autophagy in White Adipose Tissue

We investigated changes in white adipose tissue in C57BL/6J mice fed a high-fat diet (HFD). Among the white adipose tissues, we selected epididymal white adipose tissue (eWAT), which is recognized as visceral adipose tissue, and inguinal white adipose tissue (iWAT), which is recognized as subcutaneous adipose tissue, for analysis[13] (Figure 1A). In the HFD group, body weight, iWAT weight, and eWAT weight were all increased at 1 month. The differences in body weight and iWAT weight between the HFD group and the normal diet (ND) group persisted for up to 6 months, but the difference in eWAT weight disappeared at 6 months (Figure 1B). Regarding liver pathology, 2 months of HFD feeding did not induce elevated serum alanine aminotransferase levels (ALT) or histologic changes in the liver (Figure 1C and D). However, 4 months of HFD feeding induced elevated serum ALT levels, increased liver weights, and liver steatosis. In addition, 6 months of HFD feeding induced mild fibrosis in the liver (Figure 1C and D).

Next, we analyzed iWAT and eWAT after 2 months of HFD feeding in mice that exhibited iWAT and eWAT weight gain without liver steatosis. The levels of the autophagy substrate p62 decreased in both iWAT and eWAT without changes in mRNA levels (Figure 1E and F). Autophagy flux, as determined by an ex vivo assay, was increased in both

iWAT and eWAT in HFD-fed mice (Figure 1G). These results suggested that HFD feeding promoted autophagy in both types of white adipose tissue. Among autophagy-related proteins, phospho-mammalian target of rapamycin (mTOR) and phospho-p70S6k exhibited increased expression in iWAT and eWAT in mice fed an HFD compared with mice fed an ND (Figure 1E), suggesting that the autophagy promotion in the white adipose tissues of the mice fed HFD was not due to alteration of the mTOR pathway, which negatively regulates autophagy.[14] On the other hand, the levels of Rubicon, which also negatively regulates autophagy,[9] were decreased by HFD feeding in both iWAT and eWAT. The mRNA levels of Rubicon were also decreased (Figure 1E and F).

Promotion of Adipocyte Autophagy Accelerates Lipolysis in Cultured Adipocytes

To clarify the effect of lipid loading on autophagy and lipolysis in adipocytes, we evaluated autophagy flux and lipolysis after the administration of palmitic acid for 12 hours in differentiated murine adipocytes (3T3-L1 cells). Palmitic acid increased both autophagy flux and lipolysis in 3T3-L1 cells (Figure 2A). Next, to elucidate the effects of autophagy promotion of adipose tissue in lipolysis, autophagy was promoted by the administration of rapamycin or culture with starvation medium. After the administration of rapamycin for 12 hours, the autophagy flux index in 3T3-L1 cells was increased (Figure 2B). In addition, rapamycin increased the lipolysis ratio and decreased lipid accumulation, suggesting that autophagy promotion accelerates lipolysis (Figure 2B). Starvation medium also increased the autophagy flux index and lipolysis ratio and decreased lipid accumulation in 3T3-L1 cells (Figure 2C).

Adipocyte-Specific Atg7 Knockout Increases iWAT Weight and Decreases eWAT Weight With HFD Feeding

To investigate the effect of HFD feeding-induced autophagy promotion in white adipose tissue on obesity and liver steatosis, we generated adipocyte-specific Atg7-knockout (KO) mice (Adipoq-Atg7 KO mice). In iWAT and eWAT in Adipoq-Atg7 KO mice, the accumulation of p62 and the loss of LC3-II were observed along with Atg7 deficiency (Figure 3A). Under physiological conditions, there were no remarkable differences between Adipoq-Atg7 KO mice and
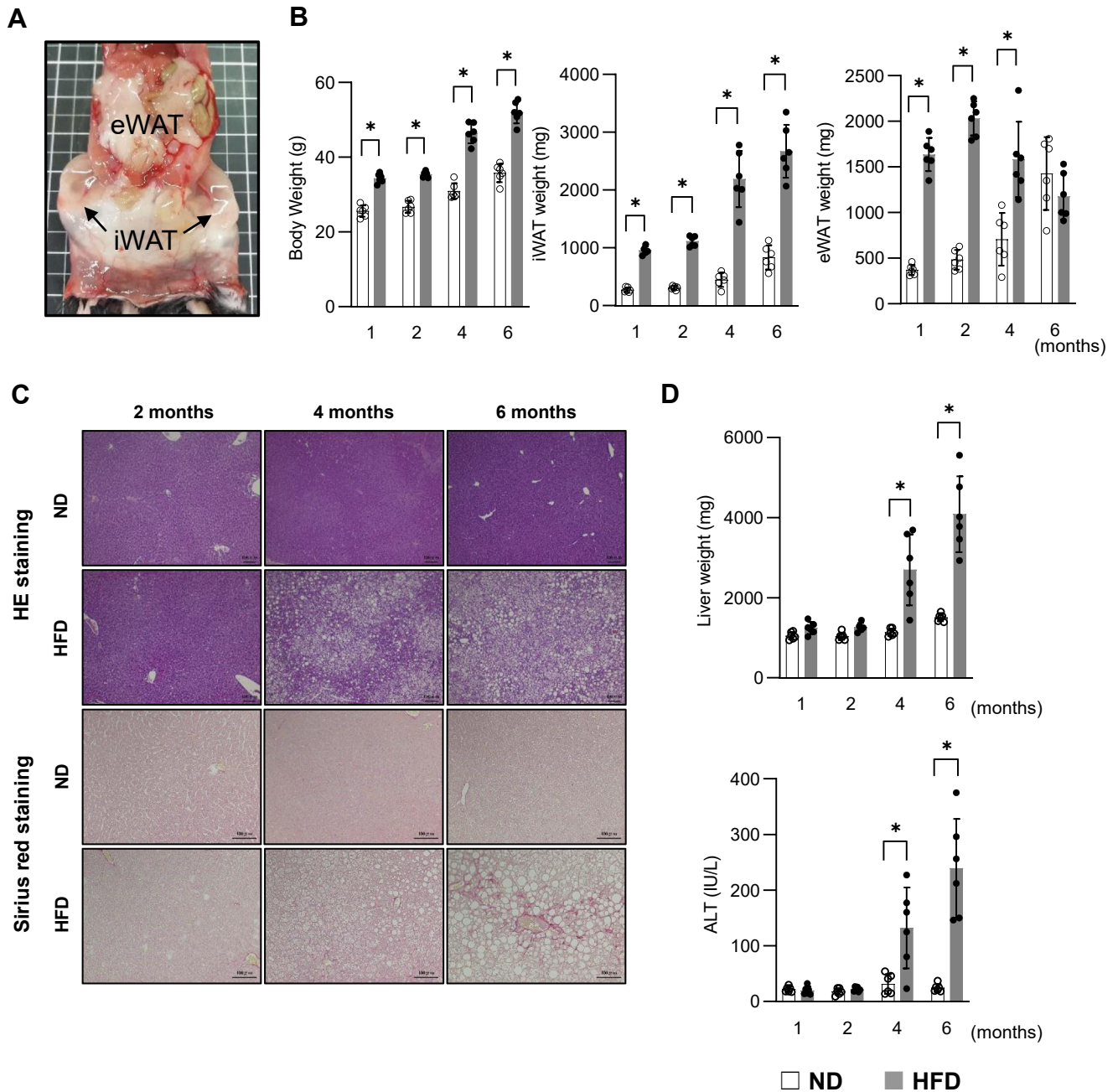
Figure 1. HFD promotes autophagy in mouse white adipose tissue. Six-week-old C57BL/6J male mice were fed an ND or HFD. (*A*) Appearance of eWAT and iWAT in C57BL/6J mice. (*B*) Changes in body weight, iWAT weight, and eWAT weight in mice fed an ND or HFD for 1–6 months. (*C*) Changes in histologic findings of H&E staining and Sirius red staining of the liver in these mice. (*D*) Changes in liver weights and serum ALT levels in these mice (n = 6 per group). (*E*) Total proteins from wild-type mice fed an ND or HFD for 2 months were analyzed by Western blotting for autophagy-related genes using Gapdh as a loading control (n = 4 per group). (*F*) The mRNA expression levels of iWAT and eWAT in wild-type mice fed an ND or HFD for 2 months for autophagy-related genes (n = 6 per group). (*G*) Autophagy flux of iWAT and iWAT in wild-type mice fed an ND or HFD for 2 months evaluated by ex vivo assay. *$P < .05$.

wild-type controls with regard to adipose tissue weights, serum free fatty acid (FFA) levels, serum cholesterol levels, serum triglyceride levels, or glucose tolerance (Figure 3B and C). Among mice fed HFD, Atg7 deficiency in adipocytes did not affect dietary intake or weight gain (Figure 4A and B). After 1 month of HFD feeding, there were significant

weight increases in both iWAT and eWAT. In iWAT, weight increases were observed even after 2 months and 4 months of HFD feeding (Figure 4B and C). On the other hand, there were no changes in eWAT weight after 2 months of HFD feeding; rather, decreases in eWAT weight were observed at later time points (Figure 4B and C). The number of small
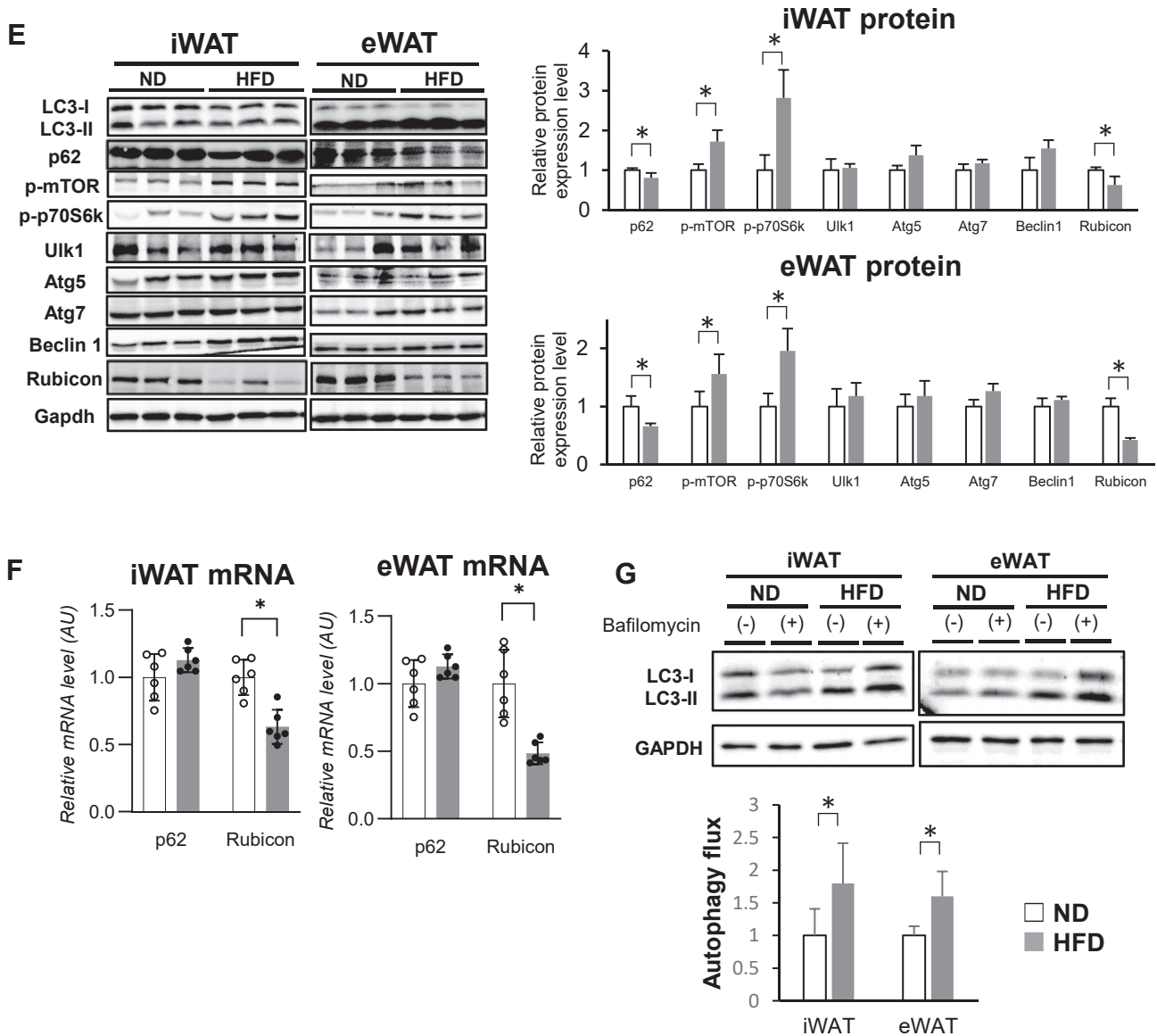
Figure 1. (*continued*).

adipocytes was decreased and the number of large adipocytes was increased in iWAT in Adipoq-Atg7 KO mice compared with wild-type controls after 2 months of HFD feeding (Figure 4D), suggesting that the decrease in lipolysis due to suppression of autophagy caused hypertrophy. In contrast, no change in adipocyte size distribution was observed in eWAT.

Adipocyte-Specific Atg7 KO Increases Apoptosis and JNK Pathway Signaling

To clarify the difference in phenotype between iWAT and eWAT after 2 months of HFD feeding, we evaluated the expression of autophagy-related genes and major genes involved in adipocyte size in iWAT and eWAT (Figure 4F and G). The accumulation of p62 and loss of

LC3-II were similarly observed in both iWAT and eWAT in Adipoq-Atg7 KO mice, suggesting that autophagy was suppressed in iWAT and eWAT. There was no change in perilipin1, which regulates adipocyte size, or lipases, including p-HSL and ATGL (Figure 4F). There were also no differences in the mRNA levels of Cd36 (a fatty acid receptor), Slc27a1 (a fatty acid transporter), Lpl (a lipase that degrades circulating triglycerides), Pparγ and Srebf1 (transcription factors involved in adipogenesis), FasN (a fatty acid synthase), and Scd1 (a stearoyl-CoA desaturase) in either iWAT or eWAT between Adipoq-Atg7 KO mice and controls (Figure 4G). Next, to elucidate whether cell death in eWAT is different from that in iWAT, the expression of proapoptotic BH3-only proteins and cleaved caspase-3 was examined. Among BH3-only proteins, Bim and phospho-Bim exhibited increased
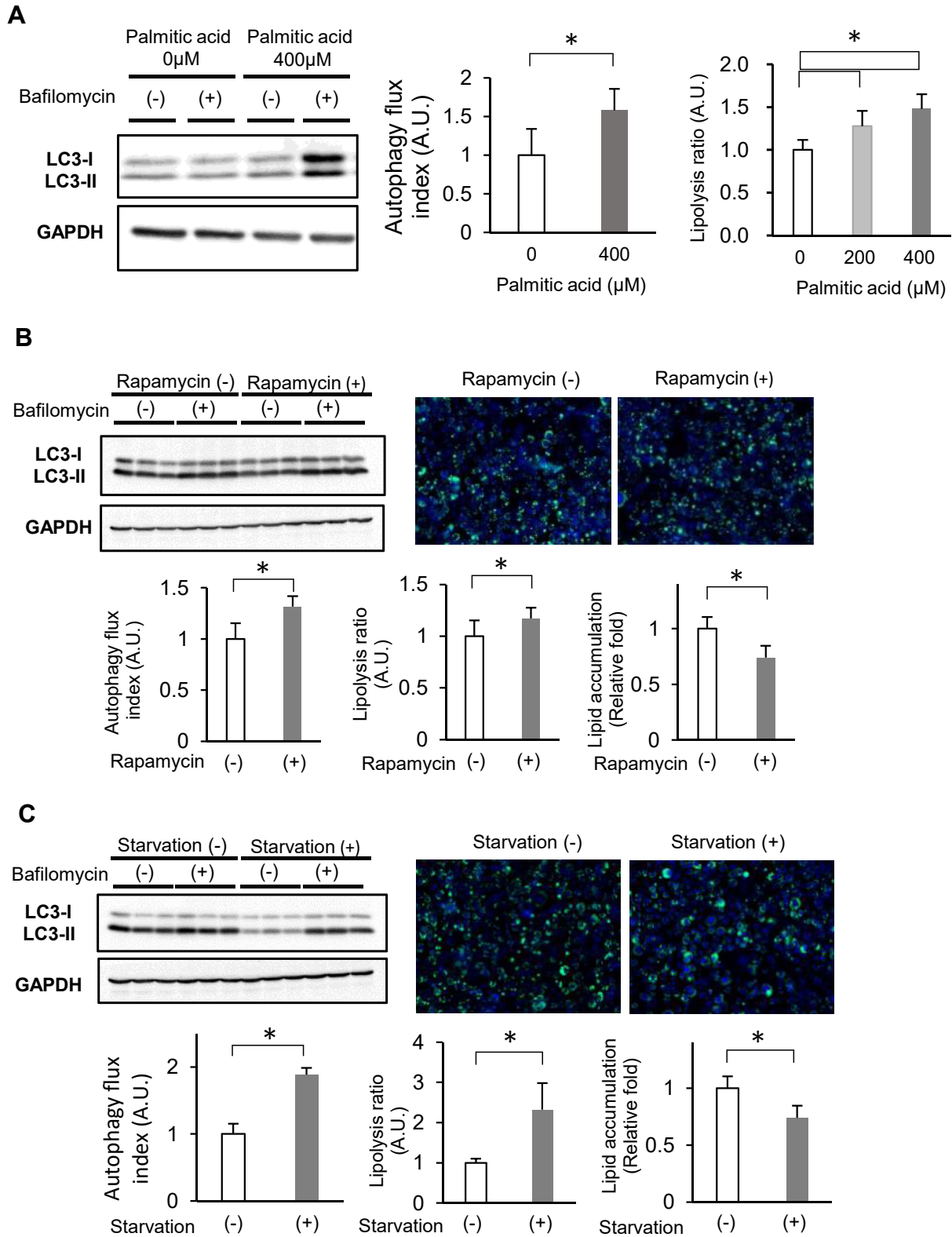
A

B

C

Figure 2. Autophagy enhancement in cultured adipocytes increases lipolysis and decreases lipid accumulation. (*A*) Autophagy flux and lipolysis ratios in differentiated 3T3-L1 cells treated with palmitic acid. (*B*) Autophagy flux, lipolysis ratios, and lipid accumulation in differentiated 3T3-L1 cells treated with rapamycin. (*C*) Autophagy flux, lipolysis ratios, and lipid accumulation in differentiated 3T3-L1 cells treated with starvation medium. *$P < .05$.
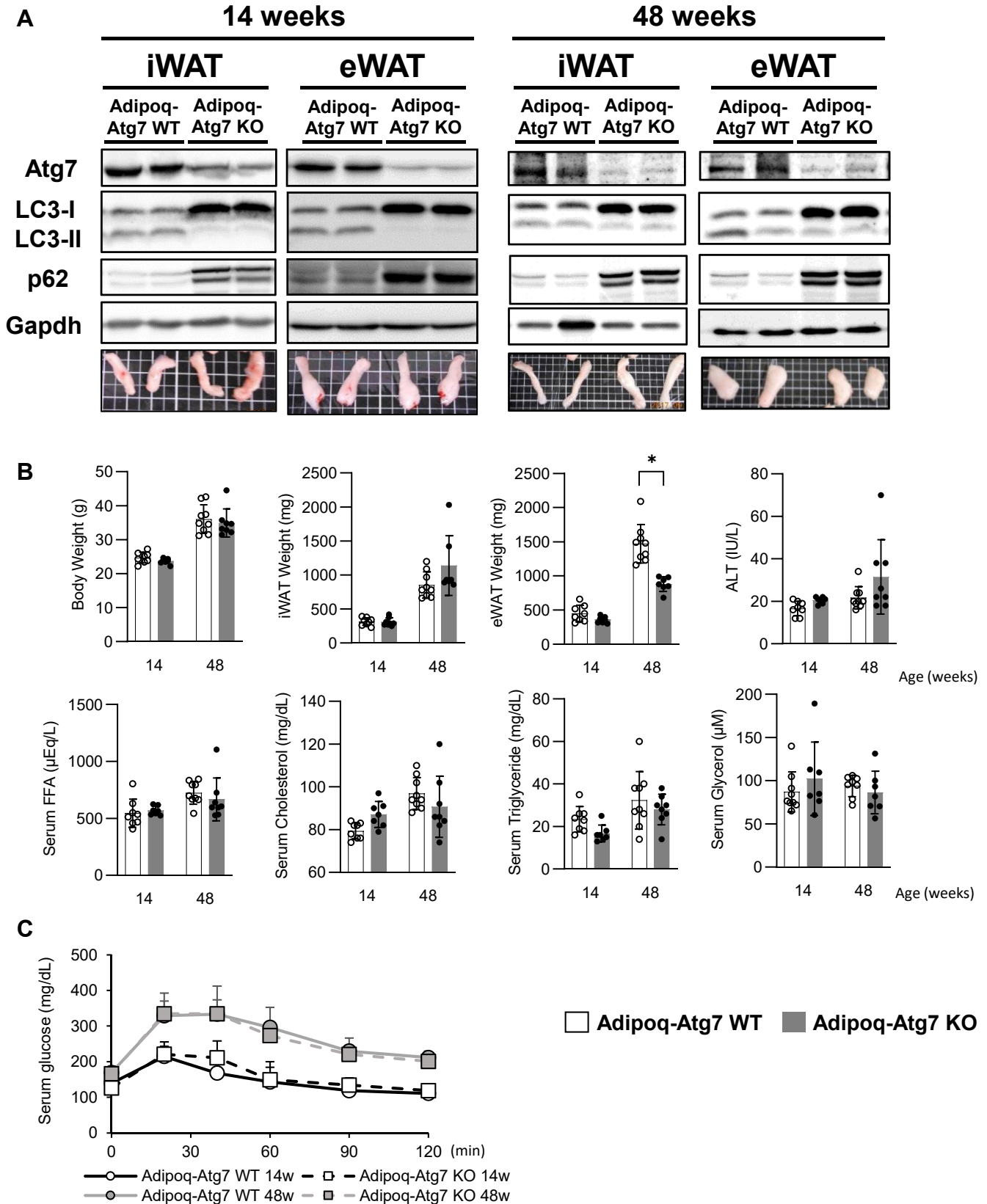
Figure 3. Adipoq-Atg7 KO mice do not show adipose tissue growth failure under ND feeding. Adipoq-Atg7 KO mice and wild-type (Adipoq-Atg7 WT) mice aged 14 weeks or 48 weeks were analyzed. (*A*) Protein expression of Atg7, p62, and LC3 and the macroscopic findings of iWAT and eWAT in these mice. (*B*) Changes in body weight, iWAT weight, eWAT weight, serum cholesterol levels, serum triglyceride levels, serum NEFA levels, serum glycerol levels, and serum ALT levels in these mice (n = 8–9 per group). (*C*) Results of glucose tolerance tests conducted on these mice 5 days before dissection. *P < .05.
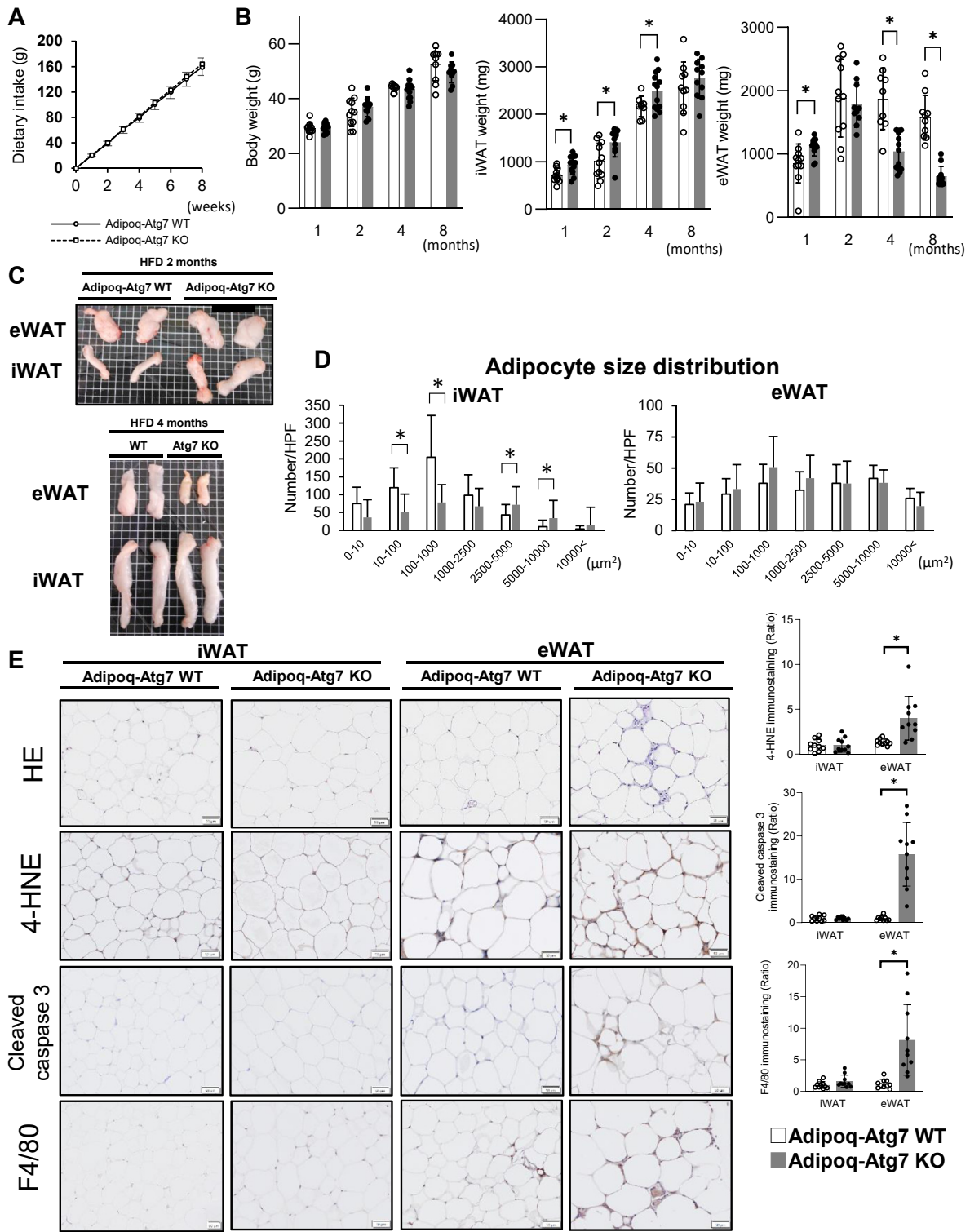
Figure 4. HFD-fed Adipoq-Atg7 KO mice show subcutaneous fat hypertrophy and visceral fat atrophy. Adipoq-Atg7 KO mice and wild-type (Adipoq-Atg7 WT) mice were fed an HFD for 1–8 months, and the adipose tissues of these mice were analyzed. (*A*) Changes in dietary intake of the 2 groups over 8 weeks (n = 9 per group). (*B*) Changes in body weight, iWAT weight, and eWAT weight (n = 8–12 per group). (*C*) Macroscopic findings of iWAT and eWAT in these mice after 2 months and 4 months of HFD feeding. (*D*) Adipocyte size distributions of iWAT and eWAT in these mice after 2 months of HFD feeding (n = 8 per group). (*E*) H&E staining, 4-HNE staining, cleaved caspase-3 staining, and F4/80 staining of iWAT and eWAT in these mice after 2 months of HFD feeding. (*F*) Protein expression levels in iWAT and eWAT of these mice after 2 months of HFD feeding were analyzed by Western blotting. (*G*) The mRNA expression levels in iWAT and eWAT of these mice after 2 months of HFD feeding were analyzed by real-time quantitative PCR. (*G*) *$P < .05$. HPF, high-power field.
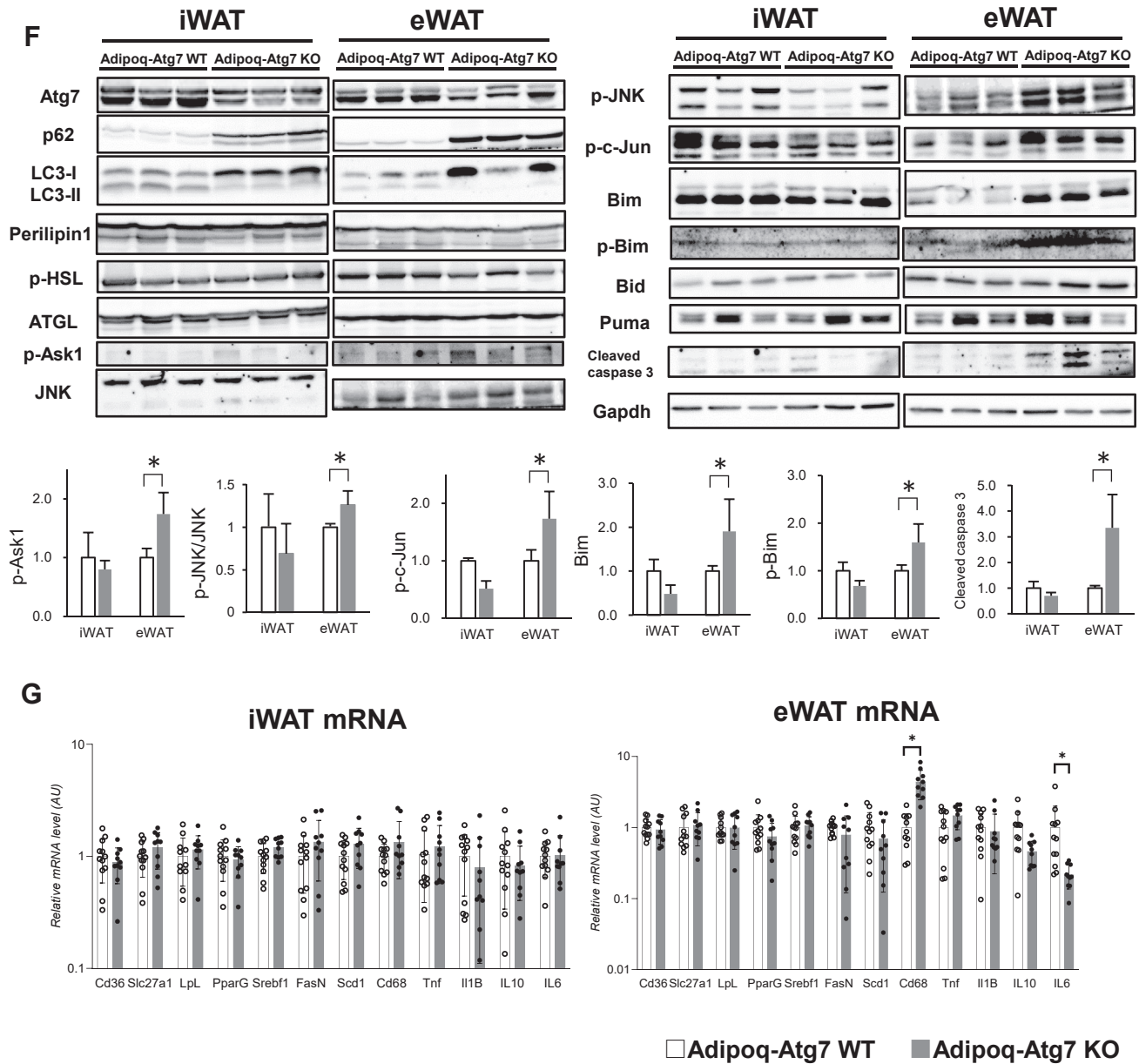
Figure 4. (*continued*).

expression levels in eWAT but not in iWAT in Adipoq-Atg7 KO mice compared with wild-type controls (Figure 4F). Cleaved caspase-3 expression levels were also increased in the eWAT of Adipoq-Atg7 KO mice compared with those of wild-type controls (Figure 4E and 4F), suggesting that adipocyte apoptosis may have been induced in eWAT. Bim is regulated by the JNK pathway,[15] and we evaluated JNK signaling pathway molecules. Atg7 deficiency increased the levels of JNK signaling pathway members, including p-Ask1, p-JNK, and p-c-Jun, which regulate Bim expression, in eWAT (Figure 4F). 4-Hydroxynonenal (4-HNE) expression was increased only in eWAT but not in iWAT of Adipoq-Atg7 KO mice compared with wild-type controls (Figure 4E),

suggesting that oxidative stress is enhanced in Adipoq-Atg7 KO mice only in eWAT.

Because apoptotic cells are engulfed mainly by macrophages, we examined macrophage infiltration in eWAT after HFD feeding. Cd68 mRNA levels were higher and F4/80-positive cells were more abundant in eWAT of Adipoq-Atg7 KO mice than in that of wild-type controls, suggesting that macrophage infiltration was increased in the eWAT of Adipoq-Atg7 KO mice (Figure 4E and G). On the other hand, there were no differences in tumor necrosis factor (TNF) α, interleukin (IL) 1B, or IL10 mRNA levels in either iWAT or eWAT between Adipoq-Atg7 KO mice and controls (Figure 4G). IL6 mRNA levels were decreased in the eWAT of Adipoq-Atg7 KO mice (Figure 4G). These results

suggested that inflammatory macrophages were not increased in eWAT in Adipoq-Atg7 KO mice, although macrophages increased.

Adipocyte-Specific Atg7 KO Decreases Serum FFA Levels and Attenuates HFD Feeding-Induced Steatosis, Liver Injury, and Liver Fibrosis

Serum FFA levels after 2 months of HFD feeding were lower in Adipoq-Atg7 KO mice than in wild-type mice (Figure 5A). There were no differences in serum cholesterol levels, serum triglyceride levels, or serum glycerol levels between Adipoq-Atg7 KO mice and wild-type controls (Figure 5A). Compared with wild-type controls, among insulin signaling pathway proteins, IRS2 levels of iWAT were higher, whereas IRS2 levels and the pAkt/Akt ratio in eWAT were lower in Adipoq-Atg7 KO mice (Figure 5B), suggesting that insulin sensitivity increased in iWAT but decreased in eWAT in Adipoq-Atg7 KO mice compared with wild-type controls. On the other hand, the expression of insulin signaling pathway proteins was not different in the liver in Adipoq-Atg7 KO mice compared with wild-type controls (Figure 5B). There were no differences in glucose tolerance between Adipoq-Atg7 KO mice and wild-type controls (Figure 5C).

Atg7 recombination was not detected in livers of Atg7 after 8 months of HFD feeding (Figure 6A). There were no changes in liver expression levels of Atg7, p62, or LC3 or hepatocyte autophagy flux between HFD-fed Adipoq-Atg7 KO mice and HFD-fed wild-type controls (Figure 6B and C). Liver weights and serum ALT levels were decreased in Adipoq-Atg7 KO mice fed HFD (Figure 6D and E). The areas of Oil Red O staining in the liver, which reflect the degree of liver lipid accumulation, were smaller in Adipoq-Atg7 KO mice than in wild-type mice after 2 months of HFD feeding (Figure 6D and F). Liver triglyceride levels were also decreased after 4 months of HFD feeding in Adipoq-Atg7 KO mice (Figure 6F). In addition, the mRNA levels of FasN and Scd1, which are fatty acid synthases, were significantly decreased in the livers of Adipoq-Atg7 KO mice (Figure 6F). The histologic findings of H&E staining after 8 months of HFD feeding revealed that Adipoq-Atg7 KO mice exhibited less lobular inflammation than wild-type mice (Figure 6D and G). The numbers of deoxyuride-5'-triphosphate biotin nick end labeling (TUNEL)–positive hepatocytes were significantly decreased in HFD-fed Adipoq-Atg7 KO mice (Figure 6D and G). In addition, the areas of Sirius red staining in the liver, which reflect liver fibrosis, and the expression levels of fibrosis-related proteins decreased in Adipoq-Atg7 KO mice compared with wild-type mice after 8 months of HFD feeding (Figure 6H).

Discussion

Although the importance of adipose tissue/liver cross-talk in NAFLD/NASH is widely recognized,[5] the role of adipose tissue in the pathogenesis of NAFLD/NASH has not been fully investigated. In the present study, we demonstrated that autophagy in adipose tissue is involved in the pathogenesis of NAFLD. This study improves not only fatty liver but also liver inflammation and fibrosis by targeting adipose tissue autophagy.

Our present study showed that HFD feeding enhanced autophagy in mouse white adipose tissue (Figure 1). Rubicon expression in white adipose tissue was decreased in HFD-fed mice compared with ND-fed mice (Figure 1E), which may have contributed to autophagy promotion in white adipose tissue. In an in vitro study, palmitic acids promoted autophagy, which induced lipolysis (Figure 2). These results suggest that HFD feeding-induced autophagy promotion causes lipolysis in white adipose tissue. Consistent with our study, some previous studies have indicated that white adipose tissue in obese rodents and humans shows not only autophagy enhancement[16–19] but also lipolysis enhancement.[20–22] Furthermore, it has been reported that lipolysis in adipocytes can be enhanced by decreasing the expression of perilipin[23] or enhancing the expression of TNFα.[24,25] However, in the present study, autophagy suppression in white adipose tissue did not change perilipin or TNFα expression, but it did affect lipid accumulation (Figure 4F and G). The findings suggest that the regulation of lipolysis by autophagy in white adipose tissue is independent of perilipin and TNFα.

In the present study, autophagy suppression in both subcutaneous fat and visceral fat induced decreased serum FFA levels. On the basis of a previous report that serum FFAs are strongly affected by subcutaneous fat lipolysis rather than visceral fat lipolysis,[26] the decreases in serum FFAs caused by Atg7 KO in adipocytes in the present study may have been affected more by subcutaneous fat than by visceral fat. On the other hand, serum FFA levels contribute to liver steatosis.[27] Genetically modified mice unable to store lipids in adipose tissue show elevated FFA levels and exacerbation of liver steatosis.[28,29] On the basis of these reports, the decreases in serum FFAs caused by Atg7 KO in adipocytes in the present study likely contributed to the attenuation of liver pathology.

Adipoq-Atg7 KO mice exhibited a characteristic phenotype of hypertrophy of subcutaneous fat and atrophy of visceral fat. Decreased Oil Red O staining in the liver was observed (after 2 months of HFD feeding) even before eWAT atrophy occurred in Adipoq-Atg7 KO mice (after 4 months of HFD feeding), suggesting that there was less involvement of eWAT atrophy in the improvement of liver steatosis. Together with the finding that increased lipid storage in iWAT and reduced serum FFA levels were observed in Adipoq-Atg7 KO mice after 2 months of HFD feeding, it is considered that the flow of fatty acids into the liver decreased as a result of the increase in lipids that can be continuously stored in iWAT, which led to the improvement of liver steatosis, liver injury, and liver fibrosis. Regarding subcutaneous fat hypertrophy and visceral fat atrophy, several drugs, such as thiazolidinediones and LXR agonists, have been reported to cause subcutaneous fat hypertrophy and visceral fat atrophy, but the underlying mechanisms are still unknown.[30,31] Okuno et al[32] reported that fat reactive oxygen species-manipulated mice showed subcutaneous fat hypertrophy and visceral fat atrophy, and the difference was due to differences in antioxidant
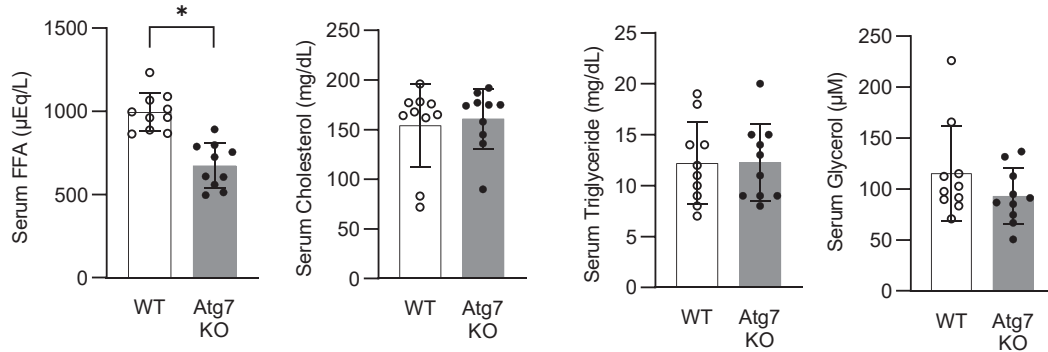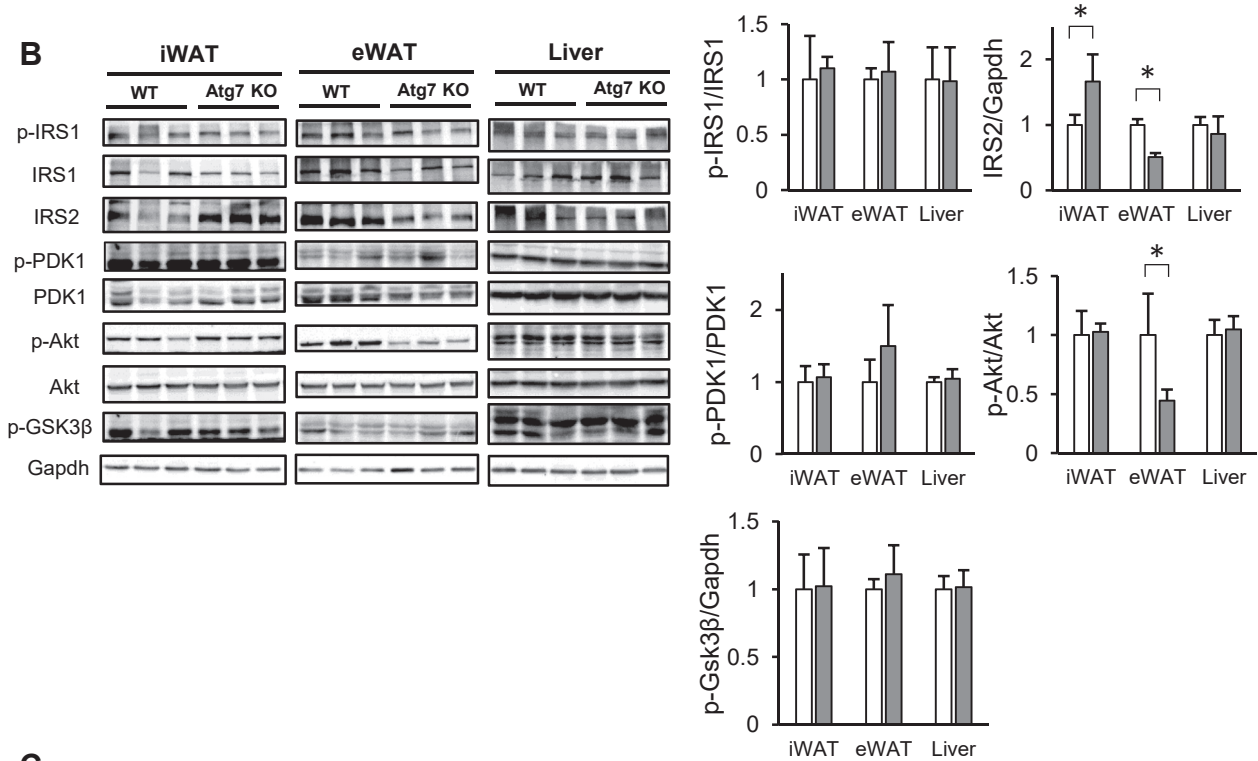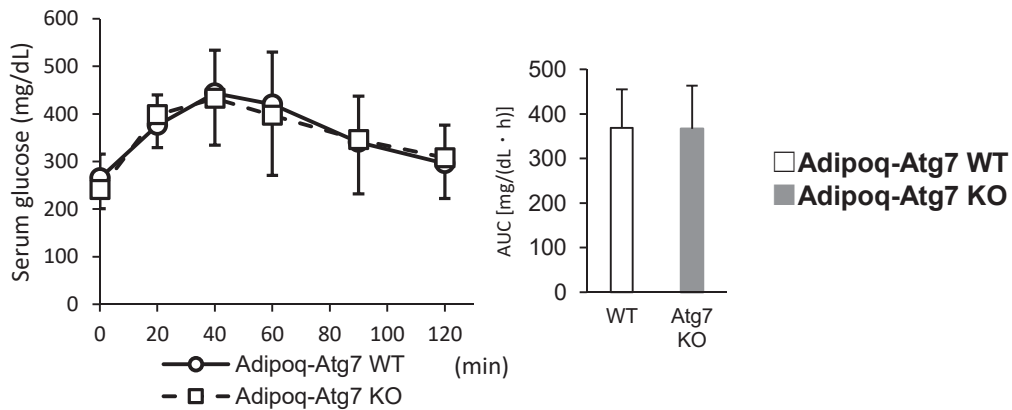
Figure 5. Serum FFA levels were decreased, while no change of glucose tolerance in HFD-fed Adipoq-Atg7 KO mice.
Adipoq-Atg7 KO mice and wild-type (Adipoq-Atg7 WT) mice were fed an HFD for 2 months, and the serum markers of these mice were analyzed (n = 10 per group). (*A*) Serum FFA levels, serum cholesterol levels, serum triglyceride levels, and serum glycerol levels in these mice. (*B*) Protein expression levels in iWAT, eWAT, and the liver of these mice after 2 months of HFD feeding were analyzed by Western blotting. (*C*) Results of glucose tolerance test conducted 5 days before dissection of these mice. AUC, area under the curve. *P < .05.
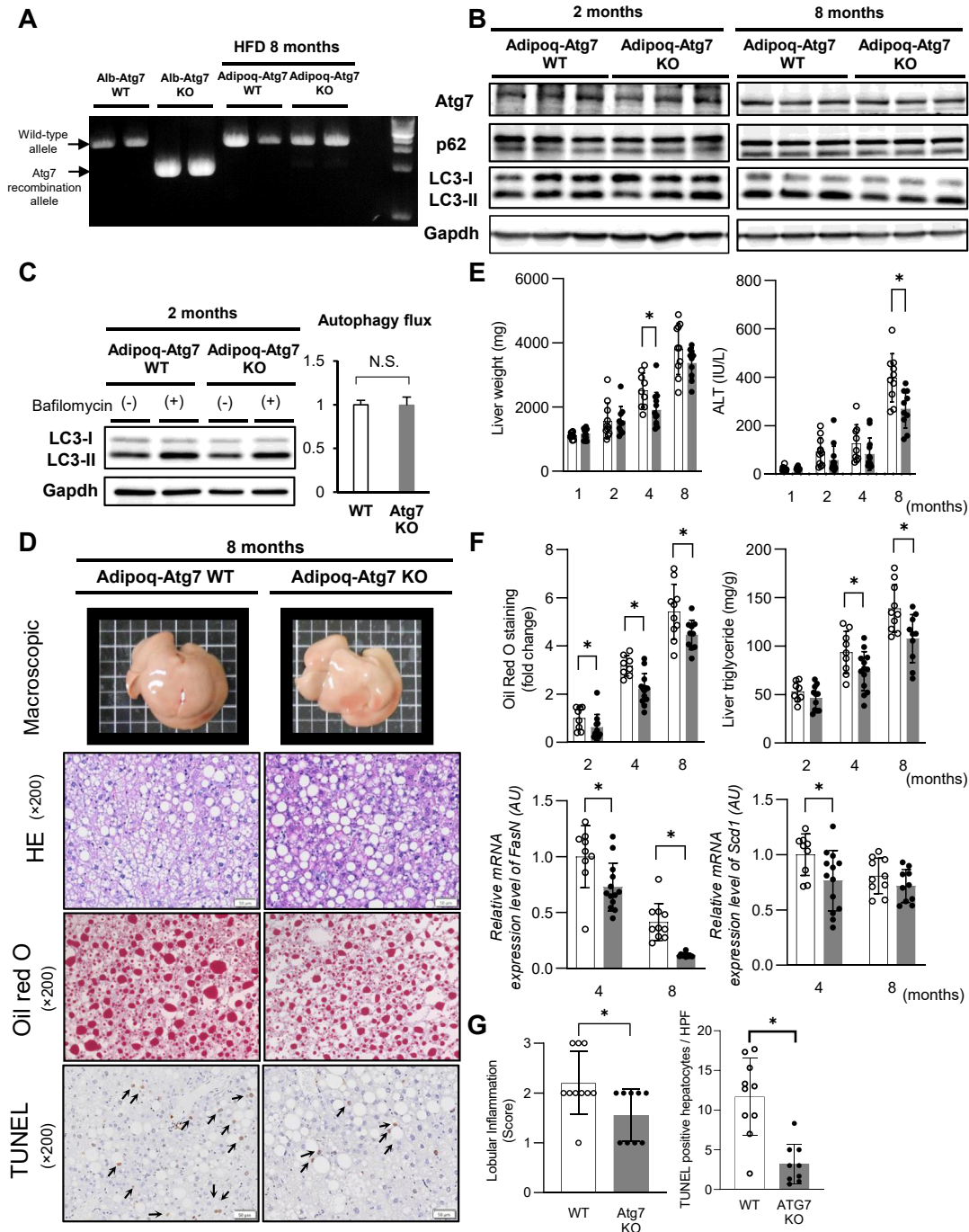
Figure 6. Adipocyte-specific Atg7 KO ameliorates liver steatosis, injury, and fibrosis resulting from HFD feeding.
Adipoq-Atg7 KO mice and wild-type (Adipoq-Atg7 WT) mice were fed an HFD for 1–8 months, and the livers of these mice were analyzed (n = 8–12 per group). (A) Liver genomic DNA from Adipoq-Atg7 KO mice and wild-type (Adipoq-Atg7 WT) mice after 8 months of HFD feeding was amplified by PCR using primers designed to flank the floxed region. An amplicon of liver genomic DNA from Albumin-Cre Atg7 fl/fl mice (Alb-Atg7 KO) was used as a reference of Atg7 recombination allele and an amplicon from wild-type mice (Alb-Atg7 WT) as a reference of wild-type allele. (B) Protein expression levels in the liver of these mice fed an HFD for 2 months or 8 months. (C) Autophagy flux of the liver in these mice after 2 months of HFD feeding. (D) Findings in the livers of these mice after 8 months of HFD feeding. Results of macroscopic examination, H&E staining (original magnification, ×200), Oil Red O staining (original magnification, ×200), and TUNEL staining (original magnification, ×200) are shown. *Arrows* indicate TUNEL-positive hepatocytes. (E) Changes in liver weights and serum ALT levels. (F) Changes in lipid accumulation in the livers of these mice. Oil Red O staining, liver triglyceride levels, and liver FasN and Scd1 mRNA levels are shown. (G) Liver inflammation and liver injury as evaluated by TUNEL-positive hepatocytes in these mice after 8 months of HFD feeding. (H) Liver fibrosis as evaluated by Sirius red staining (original magnification, ×40 and ×200) of the liver in these mice after 8 months of HFD feeding. The mRNA expression of fibrosis-related genes in the liver in these mice. *$P < .05$.
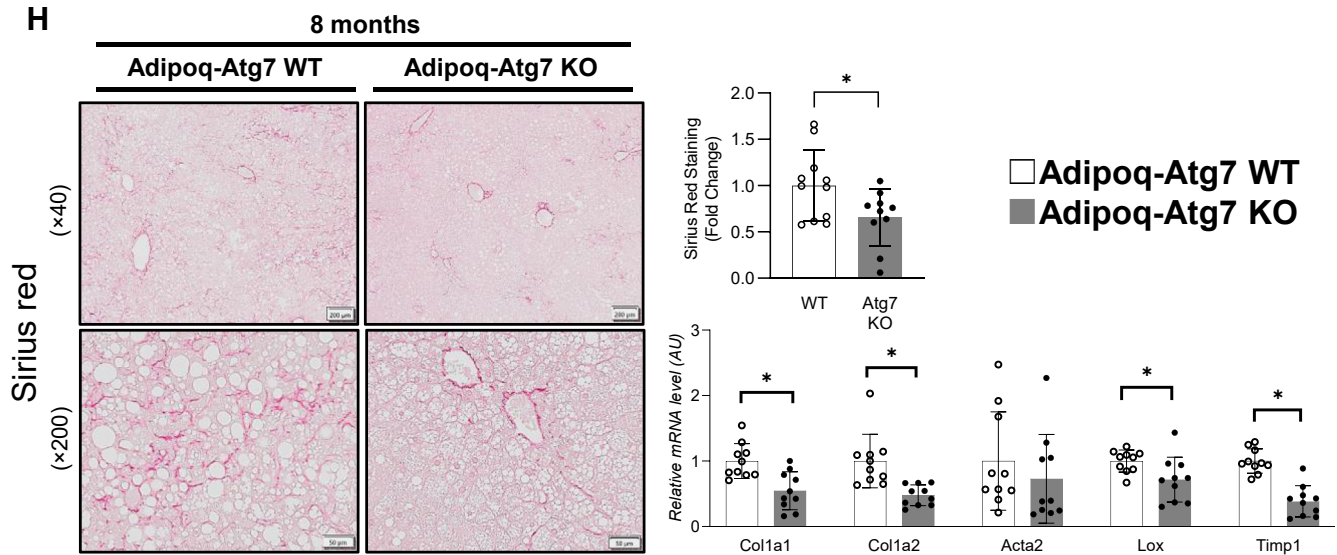
H

Figure 6. (*continued*).

sensitivity among fat depots. In our study, autophagy suppression in white adipose tissue increased Bim and cleaved caspase-3 expression only in eWAT, suggesting that inhibition of eWAT autophagy impaired adipocyte homeostasis and caused apoptosis, leading to eWAT atrophy. In addition, oxidative stress and JNK activation, which increase Bim, were enhanced in eWAT but not in iWAT in Adipoq-Atg7 KO mice, which is consistent with a previous report that oxidative stress is greater in visceral fat than in subcutaneous fat.[33] Taken together, these results suggest that in eWAT in Adipoq-Atg7 KO mice, increased oxidative stress activates the JNK pathway, which causes adipocyte apoptosis via Bim.

Most of the inflammatory cytokines in adipose tissue, such as TNFα and IL6, are produced by infiltrating macrophages.[34] The infiltration of macrophages producing inflammatory cytokines in adipose tissue exacerbates hepatic inflammation.[35] In the present study, macrophages in eWAT were increased in Adipoq-Atg7 KO mice compared with wild-type mice (Figure 4*E* and *G*). However, the expression of TNFα and IL6 in eWAT did not increase (Figure 4*G*). The results suggest that macrophage infiltration in eWAT of Adipoq-Atg7 KO mice appears in response to apoptotic adipocytes and plays a role only in the process of phagocytosis of apoptotic cells but likely does not contribute to the promotion of inflammation and does not play a considerable role in the exacerbation of liver pathogenesis.

In conclusion, autophagy was enhanced in white adipose tissues of HFD-fed mice. The suppression of autophagy in white adipose tissue ameliorated liver steatosis and fibrosis and decreased serum FFA levels via adipose-liver crosstalk. These findings indicate that adipocyte autophagy contributes to the liver pathogenesis of NAFLD. The present study suggests that autophagy in adipose tissue may be a new therapeutic target for improving the liver pathogenesis of NAFLD/NASH.

Materials and Methods

Mouse Experiments

Six-week-old male mice were used in all experiments. C57BL/6J mice and Adiponectin-Cre mice (Adipoq-Cre mice) were obtained from Charles River Laboratories (Wilmington, MA). Atg7 flox mice were obtained from Dr Komatsu (Juntendo University).[36] Adiponectin-Cre Atg7 flox/flox mice (Adipoq-Atg7 KO mice) were generated by crossing Adipoq-Cre mice and Atg7 flox mice. The mice were back-crossed with C57BL/6J mice to ensure a homogeneous background. We used Adipoq-Atg7 KO mice and littermate floxed mice as wild-type controls (Adipoq-Atg7 wild-type mice). Adipoq-Atg7 KO mice and wild-type controls were cohoused. The mice were fed either HFD containing 32% fat (HFD32; CLEA Japan, Tokyo, Japan) or a control diet (ND; CRF-1; Oriental Yeast Company, Tokyo, Japan) for 1–8 months. The mice were maintained under 12-hour light/12-hour dark cycles and treated with protocols approved by the Animal Care and Use Committee of the Graduate School of Medicine, Osaka University (Osaka, Japan). Glucose tolerance tests were performed after 8 hours of fasting 5 days before death. The mice were killed at the end of the study after 8 hours of fasting. At dissection, iWAT, eWAT, and the liver were removed as previously reported.[37] Blood samples were collected from the mouse hearts. Serum was separated by centrifugation at 13,500 rpm at room temperature for 30 minutes. Serum ALT, total cholesterol, triglyceride, FFA, and glucose levels were measured at the Oriental Yeast Company Nagahama Life Science Laboratory (Nagahama, Japan). Serum glycerol levels were measured with a Glycerol Colorimetric Assay Kit (Cayman Chemical, Ann Arbor, MI). All animals received humane care according to the criteria outlined in the "Guide for the Care and Use of

Laboratory Animals" prepared by the National Academy of Sciences and published by the National Institutes of Health.

In Vitro Study

3T3-L1 cells (JCRB9014) were obtained from the Japanese Collection of Research Bioresources Cell Bank (Osaka, Japan). Differentiated 3T3-L1 cells were generated as follows. First, cells were cultured in low-glucose Dulbecco modified Eagle medium (catalog number 08456-36; Nacalai Tesque, Kyoto, Japan) containing 10% fetal bovine serum and 1% penicillin-streptomycin. Two days after reaching confluence, the cells were cultured in differentiation medium containing 0.5 mmol/L 3-IBMX (catalog number I7018; Sigma-Aldrich, St Louis, MO), 1 μmol/L dexamethasone (catalog number D4902; Sigma-Aldrich), and 5 μmol/L insulin (catalog number I1882; Sigma-Aldrich) for 48 hours. Finally, the cells were incubated for 5 days with maintenance medium containing 5 μmol/L insulin. The degree of differentiation was confirmed by assessment of Fabp4 mRNA levels.

Rapamycin (catalog number R0395; Sigma-Aldrich) was added to cells at a final concentration of 100 μmol/L. Hanks' balanced salt solution (catalog number H6648; Sigma-Aldrich) was used as starvation medium. Palmitic acid (catalog number P0500; Sigma-Aldrich) was dissolved in a 10% bovine serum albumin solution (fatty acid-free) (catalog number A6003; Sigma-Aldrich) and administered to the cells at a final concentration of 200 or 400 μmol/L. To evaluate autophagy flux, cells were incubated for 6 hours in medium with or without 125 μmol/L bafilomycin A1 (catalog number BVT-0252-C100; BioViotica, Dransfeld, Germany) and subjected to Western blotting. The autophagy flux index was calculated as follows: autophagy flux index = (LC3-II expression level with bafilomycin A1)/(LC3-II expression level without bafilomycin A1).

To evaluate the degree of lipolysis in the experiments shown in Figure 3C, the supernatant was collected, and the glycerol concentration was measured using a glycerol colorimetric assay kit. The lipolysis ratio was calculated as the glycerol level in treated medium/glycerol level in control medium. To evaluate the degree of lipolysis in the experiments shown in Figure 2B and C, the supernatant was collected, and the nonesterified fatty acid (NEFA) concentration was measured using a NEFA C Test Wako (catalog number 279-75401; FUJIFILM Wako Pure Chemical Corporation, Osaka, Japan). The lipolysis ratio was calculated as the NEFA level in treated medium/NEFA level in control medium. To evaluate lipid accumulation, cells were stained with BODIPY493/503 (4,4-difluoro-1,3,5,7,8-pentamethyl-4-bora-3a,4a-diaza-s-indacene) (catalog number D3922; Thermo Fisher Scientific, Waltham, MA) and Hoechst 33342 (catalog number H3570; Thermo Fisher Scientific). Images were acquired with a BZ-X700 (Keyence, Osaka, Japan), and the green fluorescent areas were measured.

Ex Vivo Autophagy Flux Assay

Approximately 50 mg of iWAT and eWAT was excised and incubated in 1000 μL of medium with or without 250 μmol/L bafilomycin A1 for 24 hours at 37°C and subjected to Western blotting. The autophagy flux index was calculated as described in the in vitro study.

Autophagy Flux Assay by Primary Hepatocytes

Primary hepatocytes were isolated by two-step pronase-collagenase perfusion of mouse livers as previously reported.[38] Primary hepatocytes were maintained in William's Eagle medium and GlutaMAX Supplement (catalog number 32551020; Thermo Fisher Scientific) containing 10% fetal calf serum, 100 nmol/L insulin, and 100 nmol/L dexamethasone. To evaluate autophagy flux, cells were incubated for 2 hours in medium with or without 125 μmol/L bafilomycin A1 and subjected to Western blotting. The autophagy flux index was calculated as described in the in vitro study.

Western Blotting

Tissues were homogenized and lysed in RIPA buffer (50 mmol/L Tris-HCl, 150 mmol/L NaCl, 1% Nonidet P40 substitute, 0.5% sodium deoxycholate, 0.1% sodium dodecyl sulfate) on ice for 20 minutes. Adipose tissue samples were centrifuged at 16,000g for 20 minutes. The first supernatants without a lipid layer were collected and then centrifuged at 16,000g for 20 minutes again. Liver samples were centrifuged at 16,000g for 30 minutes once. The final supernatants were then collected. Equal amounts of total protein from different samples were subjected to sodium dodecyl sulfate-polyacrylamide gel electrophoresis. After blocking the membranes with Blocking One (catalog number 03953-95; Nacalai Tesque, Kyoto, Japan), the membranes were washed with Tris-buffered saline plus 0.1% Tween 20 (TBST) and incubated with primary antibodies in Can Get Signal Immunoreaction Enhancer Solution 1 (catalog number NKB-101; Toyobo, Osaka, Japan) at 4°C overnight. After washing with TBST, the membranes were incubated with an Amersham enhanced chemiluminescence antibody (catalog number NA934; GE Healthcare, Chicago, IL) in Can Get Signal Immunoreaction Enhancer Solution 2 (catalog number NKB-101; Toyobo). Super Signal West Pico PLUS Chemiluminescent Substrate (catalog number 34580; Thermo Fisher Scientific) was used for luminescence analysis. The bands were detected, and the protein expression levels were quantified using Fusion Solo S (Vilber Lourmat, Collegien, France). The levels of each protein were normalized to the Gapdh levels. The antibodies used for immunodetection are listed in Table 1.

Real-Time Reverse Transcription Polymerase Chain Reaction Analysis

Total RNA was extracted from tissue using an RNeasy Lipid Tissue Mini Kit (catalog number 74804; Qiagen, Hilden, Germany). One microgram of total RNA eluted from each sample was used for reverse transcription using a ReverTra Ace qPCR RT Kit (catalog number FSQ-101; Toyobo). The mRNA expression of specific genes was analyzed using a TaqMan Gene Expression Assay (Thermo

Table 1. List of Antibodies Used for Western Blotting Analysis

Antibody	Company	Product number
LC3B Rabbit Ab	Cell Signaling Technology (Beverly, MA)	#2775
SQSTM1/p62 (D6M5X) Rabbit Ab (Rodent Specific)	Cell Signaling Technology	#23214
Phospho-mTOR (Ser2448) (D9C2) Rabbit mAb	Cell Signaling Technology	#5536
p-p70S6 kinase(S371) Rabbit Ab	Cell Signaling Technology	#9208
ULK1 (D8H5) Rabbit mAb	Cell Signaling Technology	#8054
Atg7 Rabbit Ab	Cell Signaling Technology	#2631
Atg5 (D1G9) Rabbit mAb	Cell Signaling Technology	#8540
Beclin-1 (D40C5) Rabbit mAb	Cell Signaling Technology	#3495
Rubicon (D9F7) Rabbit mAb	Cell Signaling Technology	#8465
GAPDH (D16H11) Rabbit mAb	Cell Signaling Technology	#5174
Perilipin (D1D8) Rabbit mAb	Cell Signaling Technology	#9349
Phospho-HSL (S563) Rabbit Ab	Cell Signaling Technology	#4139
ATGL (30A4) Rabbit mAb	Cell Signaling Technology	#2439
p-Ask1 (S967) Rabbit Ab	Cell Signaling Technology	#3764
SAPK/JNK (56G8) Rabbit mAb	Cell Signaling Technology	#9258
p-SAPK/JNK (T183/Y185) (81E11) Rabbit mAb	Cell Signaling Technology	#4668
p-c-Jun (S73) (D47G9)	Cell Signaling Technology	#3270
Bim (C34C5) Rabbit mAb	Cell Signaling Technology	#2933
Phospho-Bim (Ser69) (D7E11) Rabbit mAb	Cell Signaling Technology	#4585
Bid Antibody (Mouse Specific)	Cell Signaling Technology	#2003
Puma (D7L9L) Rabbit mAb (Rodent Specific)	Cell Signaling Technology	#24633
Cleaved Caspase-3 (D175) Rabbit Ab	Cell Signaling Technology	#9661
p-IRS-1 (S612) (C15H5) Rabbit mAb	Cell Signaling Technology	#3203
IRS-1 (D23G12) Rabbit mAb	Cell Signaling Technology	#3407
IRS-2 Rabbit mAb	Cell Signaling Technology	#4502
p-PDK1 (S241) Rabbit mAb	Cell Signaling Technology	#3438
PDK1 (D37A7) Rabbit mAb	Cell Signaling Technology	#5662
p-Akt (S473) (D9E) Rabbit mAb	Cell Signaling Technology	#4060
Akt (pan) (C67E7) Rabbit mAb	Cell Signaling Technology	#4691
p-Gsk-3-β (S9) (D85E12) Rabbit mAb	Cell Signaling Technology	#5558

Fisher Scientific). All TaqMan polymerase chain reaction (PCR) probes were obtained from Thermo Fisher Scientific (Table 2).

Histologic Analysis

To produce formalin-fixed paraffin-embedded tissue sections, adipose tissue samples and liver samples were fixed in 10% neutral buffered formaldehyde solution (catalog number 37152-51; Nacalai Tesque) for 48 hours.

To produce fresh-frozen sections, liver samples were directly embedded with Tissue-Tek OCT Compound (catalog number 45833; Sakura Finetek Japan Co, Tokyo, Japan). H&E staining was performed with a standard protocol. F4/80 staining was performed with a VECTASTAIN ABC-HRP Kit, peroxidase (rat immunoglobulin G) (catalog number PK-4004; Vector Laboratories, Inc, Burlingame, CA) and a rat anti-mouse F4/80 antibody (catalog number MCA497G; Bio-Rad, Berkeley, CA). 4-HNE staining was performed with the VECTASTAIN ABC-HRP Kit, peroxidase (rabbit immunoglobulin G) (catalog number PK-4001; Vector Laboratories) and a rabbit anti-4-HNE antibody (catalog number ab46545; Abcam, Cambridge, UK). Cleaved caspase-3 staining was performed with a VECTASTAIN ABC-HRP Kit, peroxidase (rabbit immunoglobulin G) and a cleaved caspase-3 (D175) rabbit antibody (catalog number #9661; Cell Signaling Technology, Beverly, MA). In F4/80, 4-HNE and cleaved caspase-3 immunostaining, 5 visual fields of a magnified image (original magnification, $\times 200$) were randomly selected for each immunostained section, and the positive area per cell ratio was calculated. HALO software (Indica Labs, Albuquerque, NM) was used for quantitative analysis of these images. Oil Red O (FUJIFILM Wako Pure Chemical Corporation) staining was performed. TUNEL staining was performed with an ApopTag Peroxidase In Situ Apoptosis Detection Kit (catalog number S-7100; Merck, Darmstadt, Germany). Sirius red staining was performed with a Picrosirius Red Stain Kit (catalog number 24901; Polysciences, Inc, Warrington, PA). Lobular inflammation was defined by the presence of a focus of 2 or more

Table 2. List of Primers Used for Real-Time PCR

Gene	Company	Product number
Murine actin β	Thermo Fisher Scientific (Waltham, MA)	Mm02619580_g1
Murine Sqstm1 (p62)	Thermo Fisher Scientific	Mm00448091_m1
Murine 1700021 (Rubicon)	Thermo Fisher Scientific	Mm00553869_m1
Murine Cd36	Thermo Fisher Scientific	Mm00432403_m1
Murine Slc27a1 (Fatp1)	Thermo Fisher Scientific	Mm00449511_m1
Murine Lpl	Thermo Fisher Scientific	Mm00434764_m1
Murine Pparg	Thermo Fisher Scientific	Mm01184322_m1
Murine Srebf1	Thermo Fisher Scientific	Mm00550338_m1
Murine FasN	Thermo Fisher Scientific	Mm00662319_m1
Murine Scd1	Thermo Fisher Scientific	Mm00772290_m1
Murine Cd68	Thermo Fisher Scientific	Mm00839636_g1
Murine Tnf	Thermo Fisher Scientific	Mm00443258_m1
Murine IL1B	Thermo Fisher Scientific	Mm00434228_m1
Murine IL10	Thermo Fisher Scientific	Mm00439614_m1
Murine IL6	Thermo Fisher Scientific	Mm00446190_m1
Murine Col1a1	Thermo Fisher Scientific	Mm00801666_g1
Murine Col1a2	Thermo Fisher Scientific	Mm00483888_m1
Murine Asma	Thermo Fisher Scientific	Mm00725412_s1
Murine Timp1	Thermo Fisher Scientific	Mm01341361_m1
Murine Lox	Thermo Fisher Scientific	Mm00493586_m1

inflammatory cells within the lobule and was scored as follows: 0, none; 1, $<$2 foci per field; 2, 2–4 foci per field; and 3, $>$4 foci per field (original magnification, ×200). Images were acquired with a BZ-X700 (Keyence) or a VS200 (Olympus, Tokyo, Japan).

Measurement of Intrahepatic Lipids

Lipids were isolated from liver tissues via the extraction procedure of Folch et al.[39] The triglyceride level per gram of liver was measured by using a Triglyceride E Test Wako (catalog number 432-40201l; FUJIFILM Wako Pure Chemical Corporation).

Detection of Cre Recombination

Albumin-Cre mice, which express Cre recombinase under the liver-specific albumin promoter, were purchased from Jackson Laboratories (Bar Harbor, ME). Albumin-Cre Atg7 fl/fl mice were generated by crossing Albumin-Cre mice and Atg7 flox mice. The DNA was extracted from tissue using a DNeasy Blood & Tissue Kit (catalog number 69506; Qiagen). Cre-mediated recombination was confirmed by PCR with genomic DNA in the liver and primers as previously reported[40] (forward, TGGCTGCTACTTCTGCAATGATGT; reverse, CTAAGCAGGT-GAGA TCTACACTCA).

Statistical Analysis

Data are presented as the mean ± standard deviation. Comparisons between 2 groups were performed with unpaired two-sided t tests. $P <$.05 was considered indicative of statistical significance.

References

1. Eguchi Y, Wong G, Lee I-H, Akhtar O, Lopes R, Sumida Y. Hepatocellular carcinoma and other complications of nonalcoholic fatty liver disease and nonalcoholic steatohepatitis in Japan: a structured literature review article. Hepatol Res 2021;51:19–30.
2. Younossi ZM, Koenig AB, Abdelatif D, Fazel Y, Henry L, Wymer M. Global epidemiology of nonalcoholic fatty liver disease: meta-analytic assessment of prevalence, incidence, and outcomes. Hepatology 2016;64:73–84.
3. van der Poorten D, Milner K-L, Hui J, Hodge A, Trenell MI, Kench JG, London R, Peduto T, Chisholm DJ, George J. Visceral fat: a key mediator of steatohepatitis in metabolic liver disease. Hepatology 2008;48:449–457.
4. Kim D, Kim W, Joo SK, Han J, Kim JH, Harrison SA, Younossi ZM, Ahmed A. Association between body size-metabolic phenotype and nonalcoholic steatohepatitis and significant fibrosis. J Gastroenterol 2020; 55:330–341.
5. Azzu V, Vacca M, Virtue S, Allison M, Vidal-Puig A. Adipose tissue-liver cross talk in the control of whole-body metabolism: implications in nonalcoholic fatty liver disease. Gastroenterology 2020;158:1899–1912.
6. Singh R, Kaushik S, Wang Y, Xiang Y, Novak I, Komatsu M, Tanaka K, Cuervo AM, Czaja MJ. Autophagy regulates lipid metabolism. Nature 2009; 458:1131–1135.

7. González-Rodríguez A, Mayoral R, Agra N, Valdecantos MP, Pardo V, Miquilena-Colina ME, Vargas-Castrillón J, Lo Iacono O, Corazzari M, Fimia GM, Piacentini M, Muntané J, Boscá L, García-Monzón C, Martín-Sanz P, Valverde ÁM. Impaired autophagic flux is associated with increased endoplasmic reticulum stress during the development of NAFLD. Cell Death Dis 2014; 5:e1179.

8. Tanaka S, Hikita H, Tatsumi T, Sakamori R, Nozaki Y, Sakane S, Shiode Y, Nakabori T, Saito Y, Hiramatsu N, Tabata K, Kawabata T, Hamasaki M, Eguchi H, Nagano H, Yoshimori T, Takehara T. Rubicon inhibits autophagy and accelerates hepatocyte apoptosis and lipid accumulation in nonalcoholic fatty liver disease in mice. Hepatology 2016;64:1994–2014.

9. Matsunaga K, Saitoh T, Tabata K, Omori H, Satoh T, Kurotori N, Maejima I, Shirahama-Noda K, Ichimura T, Isobe T, Akira S, Noda T, Yoshimori T. Two Beclin 1-binding proteins, Atg14L and Rubicon, reciprocally regulate autophagy at different stages. Nat Cell Biol 2009;11:385–396.

10. Singh R, Xiang Y, Wang Y, Baikati K, Cuervo AM, Luu YK, Tang Y, Pessin JE, Schwartz GJ, Czaja MJ. Autophagy regulates adipose mass and differentiation in mice. J Clin Invest 2009;119:3329–3339.

11. Altshuler-Keylin S, Shinoda K, Hasegawa Y, Ikeda K, Hong H, Kang Q, Yang Y, Perera RM, Debnath J, Kajimura S. Beige adipocyte maintenance is regulated by autophagy-induced mitochondrial clearance. Cell Metab 2016;24:402–419.

12. Yamamuro T, Kawabata T, Fukuhara A, Saita S, Nakamura S, Takeshita H, Fujiwara M, Enokidani Y, Yoshida G, Tabata K, Hamasaki M, Kuma A, Yamamoto K, Shimomura I, Yoshimori T. Age-dependent loss of adipose Rubicon promotes metabolic disorders via excess autophagy. Nat Commun 2020;11: 4150.

13. Tran TT, Kahn CR. Transplantation of adipose tissue and stem cells: role in metabolism and disease. Nat Rev Endocrinol 2010;6:195–213.

14. Jung CH, Ro S-H, Cao J, Otto NM, Kim D-H. mTOR regulation of autophagy. FEBS Lett 2010; 584:1287–1295.

15. Solinas G, Becattini B. JNK at the crossroad of obesity, insulin resistance, and cell stress response. Mol Metab 2016;6:174–184.

16. Nuñez CE, Rodrigues VS, Gomes FS, Moura RF de, Victorio SC, Bombassaro B, Chaim EA, Pareja JC, Geloneze B, Velloso LA, Araujo EP. Defective regulation of adipose tissue autophagy in obesity. Int J Obes (Lond) 2013;37:1473–1480.

17. Hansson B, Wasserstrom S, Morén B, Periwal V, Vikman P, Cushman SW, Göransson O, Storm P, Stenkula KG. Intact glucose uptake despite deteriorating signaling in adipocytes with high-fat feeding. J Mol Endocrinol 2018;60:199–211.

18. Xu Q, Mariman ECM, Roumans NJT, Vink RG, Goossens GH, Blaak EE, Jocken JWE. Adipose tissue autophagy related gene expression is associated with glucometabolic status in human obesity. Adipocyte 2018;7:12–19.

19. Kovsan J, Blüher M, Tarnovscki T, Klöting N, Kirshtein B, Madar L, Shai I, Golan R, Harman-Boehm I, Schön MR, Greenberg AS, Elazar Z, Bashan N, Rudich A. Altered autophagy in human adipose tissues in obesity. J Clin Endocrinol Metab 2011;96:E268–E277.

20. Reynisdottir S, Langin D, Carlström K, Holm C, Rössner S, Arner P. Effects of weight reduction on the regulation of lipolysis in adipocytes of women with upper-body obesity. Clin Sci 1995;89:421–429.

21. Stevens J, Green MH, Kaiser DL, Pohl SL. Insulin resistance in adipocytes from fed and fasted obese rats: dissociation of two insulin actions. Mol Cell Biochem 1981;37:177–183.

22. Johnson JA, Fried SK, Pi-Sunyer FX, Albu JB. Impaired insulin action in subcutaneous adipocytes from women with visceral obesity. Am J Physiol Endocrinol Metab 2001;280:E40–E49.

23. Wang Y, Sullivan S, Trujillo M, Lee M-J, Schneider SH, Brolin RE, Kang YH, Werber Y, Greenberg AS, Fried SK. Perilipin expression in human adipose tissues: effects of severe obesity, gender, and depot. Obes Res 2003; 11:930–936.

24. Rydén M, Arvidsson E, Blomqvist L, Perbeck L, Dicker A, Arner P. Targets for TNF-alpha-induced lipolysis in human adipocytes. Biochem Biophys Res Commun 2004; 318:168–175.

25. Prins JB, Niesler CU, Winterford CM, Bright NA, Siddle K, O'Rahilly S, Walker NI, Cameron DP. Tumor necrosis factor-alpha induces apoptosis of human adipose cells. Diabetes 1997;46:1939–1944.

26. Jensen MD, Cardin S, Edgerton D, Cherrington A. Splanchnic free fatty acid kinetics. Am J Physiol Endocrinol Metab 2003;284:E1140–E1148.

27. Neuschwander-Tetri BA. Hepatic lipotoxicity and the pathogenesis of nonalcoholic steatohepatitis: the central role of nontriglyceride fatty acid metabolites. Hepatology 2010;52:774–788.

28. Kim S-J, Feng D, Guillot A, Dai S, Liu F, Hwang S, Parker R, Seo W, He Y, Godlewski G, Jeong WI, Lin Y, Qin X, Kunos G, Gao B. Adipocyte death preferentially induces liver injury and inflammation through the activation of chemokine (C-C Motif) receptor 2-positive macrophages and lipolysis. Hepatology 2019; 69:1965–1982.

29. Tanaka N, Takahashi S, Matsubara T, Jiang C, Sakamoto W, Chanturiya T, Teng R, Gavrilova O, Gonzalez FJ. Adipocyte-specific disruption of fat-specific protein 27 causes hepatosteatosis and insulin resistance in high-fat diet-fed mice. J Biol Chem 2015; 290:3092–3105.

30. Wilding J. Thiazolidinediones, insulin resistance and obesity: finding a balance. Int J Clin Pract 2006; 60:1272–1280.

31. Archer A, Stolarczyk E, Doria ML, Helguero L, Domingues R, Howard JK, Mode A, Korach-André M, Gustafsson JÅ. LXR activation by GW3965 alters fat

tissue distribution and adipose tissue inflammation in ob/ob female mice. J Lipid Res 2013;54:1300–1311.

32. Okuno Y, Fukuhara A, Hashimoto E, Kobayashi H, Kobayashi S, Otsuki M, Shimomura I. Oxidative stress inhibits healthy adipose expansion through suppression of SREBF1-mediated lipogenic pathway. Diabetes 2018;67:1113–1127.

33. Liu R, Pulliam DA, Liu Y, Salmon AB. Dynamic differences in oxidative stress and the regulation of metabolism with age in visceral versus subcutaneous adipose. Redox Biol 2015;6:401–408.

34. Weisberg SP, McCann D, Desai M, Rosenbaum M, Leibel RL, Ferrante AW. Obesity is associated with macrophage accumulation in adipose tissue. J Clin Invest 2003;112:1796–1808.

35. Bijnen M, Josefs T, Cuijpers I, Maalsen CJ, van de Gaar J, Vroomen M, Wijnands E, Rensen SS, Greve JWM, Hofker MH, Biessen EAL, Stehouwer CDA, Schalkwijk CG, Wouters K. Adipose tissue macrophages induce hepatic neutrophil recruitment and macrophage accumulation in mice. Gut 2018;67:1317–1327.

36. Komatsu M, Waguri S, Ueno T, Iwata J, Murata S, Tanida I, Ezaki J, Mizushima N, Ohsumi Y, Uchiyama Y, Kominami E, Tanaka K, Chiba T. Impairment of starvation-induced and constitutive autophagy in Atg7-deficient mice. J Cell Biol 2005;169:425–434.

37. Zhang F, Hao G, Shao M, Nham K, An Y, Wang Q, Zhu Y, Kusminski CM, Hassan G, Gupta RK, Zhai Q, Sun X, Scherer PE, Oz OK. An adipose tissue atlas: an image-guided identification of human-like BAT and beige depots in rodents. Cell Metab 2018;27:252–262.

38. Myojin Y, Hikita H, Sugiyama M, Sasaki Y, Fukumoto K, Sakane S, Makino Y, Takemura N, Yamada R, Shigekawa M, Kodama T, Sakamori R, Kobayashi S, Tatsumi T, Suemizu H, Eguchi H, Kokudo N, Mizokami M, Takehara T. Hepatic stellate cells in hepatocellular carcinoma promote tumor growth via growth differentiation factor 15 production. Gastroenterology 2021;160:1741–1754.

39. Folch J, Lees M, Sloane Stanley GH. A simple method for the isolation and purification of total lipides from animal tissues. J Biol Chem 1957;226:497–509.

40. Jung HS, Chung KW, Won Kim J, Kim J, Komatsu M, Tanaka K, Nguyen YH, Kang TM, Yoon K-H, Kim J-W, Jeong YT, Han MS, Lee M-K, Kim K-W, Shin J, Lee M-S. Loss of autophagy diminishes pancreatic beta cell mass and function with resultant hyperglycemia. Cell Metab 2008;8:318–324.

Correspondence
Address correspondence to: Tetsuo Takehara, MD, PhD, 2-2 Yamadaoka, Suita, Osaka, 565-0871 Japan. e-mail: takehara@gh.med.osaka-u.ac.jp; fax: +81-6-6879-3629.